Modeling of cutting forces in five-axis milling of sculptured surfaces directly from a CAM tool path

Yacine Hamiche (hamichey84@gmail.com)
Ecole Militaire Polytechnique https://orcid.org/0000-0003-3056-8898
Nasreddine Zeroudi
Ecole Militaire Polytechnique
Rabah Lamara
Ecole Militaire Polytechnique

Research Article

Keywords: Cutting force prediction, Five-axis milling, Analytical method, CAM toolpath, Bull-nose milling

Posted Date: April 1st, 2021

DOI: https://doi.org/10.21203/rs.3.rs-354355/v1

Modeling of cutting forces in five-axis milling of sculptured surfaces directly from a CAM tool path

Yacine Hamiche * · Nasreddine Zeroudi · Rabah Lamara
Ecole Militaire polytechnique, BP 17 Bordj El Bahri, 16111 Alger, Algérie
e-mail: hamichey84@gmail.com
e-mail: nasreddine_zeroudi@yahoo.fr
e-mail: lamara2014@ gmail.com

Abstract The present work is motivated by the fact that for predicting cutting forces, which arise under various cutting conditions, workpiece-tool pairs and machining depths, the numerical methods are slower and less efficient than the analytical methods. In addition, recent developments in Computer Assisted Machining (CAM) techniques have enabled analytical methods to be applied even with a complex workpiece geometry. The present paper presents a practical and powerful analytical method which is based on the use of the toolpath file as the main information source for the machined surface. This method takes into account tool position and orientation in a five-axis milling process with tool ball-end modeled as a sphere called bull-nose. Also assumptions are made to get a good approximation in the calculation of global and local cutting forces, in the aim of developing an analytical model able to predict the cutting forces for five-axis milling process, easy to apply for any practical case.

Keywords Cutting force prediction · Five-axis milling · Analytical method · CAM toolpath · Bull-nose milling

Nomenclature

(O, X, Y, Z)	Global reference system	(e_r, e_κ, e_ψ)	Local cutting edge base vectors
(E, x, y, z)	Tool reference system	Δp	Path interval
x_p, y_p, z_p	Curent point coordinates	P_n	Normal plane
$CL\ (i, k)$	Cutter location points	P_t	Tangent plane
$CC\ (i, k)$	Cutter contact points	θ_n	Normal rotation angle
j	Tooth index	θ_t	Tangent rotation angle
I, J, K	Unit vectors	$\theta_{z'y}$	Eliptical deformation angle
T_k	Trajectory index	δ	Local inclination angle
P	Current point	θ	Rotation angle
ψ_j	Edge location angle	N_t	Rotation number of the tool
$\Delta\psi$	Shift angle	n	Normal vector of the cutting edge
κ	e_r Vector inclination angle	f	Feed per rotation
Ω	Spindle frequency	f_t	Feed per tooth
z	Height along the rotation axis	t	Tangent vector of the cutting edge
$R(z)$	cutting radius	t_0	Undeformed chip thickness
R_0	Tool radius	$i\ (z)$	Local helix angle
R_e	Tool radial eccentricity	λ_s	Local cutting edge inclination angle

α_0	orthogonal cutting angle	γ_0	Orthogonal rake angle
α_n	normal cutting angle	γ_n	Normal rake angle
φ_x, φ_z	Local feed angles	dw	Local elementary cutting width
$\varphi_{\Delta p}$	Transverse inclination angle	C_P, R_P	Parameters of tool envelope on the previous tool path
z_{sp}	Height of the previous machined surface	F_x, F_y, F_z	Cutting force component along x, y and z
e_j	Eccentricity vector for tooth j	$F_{x'}$, $F_{y'}$, $F_{z'}$	Cutting force component along x', y' and z'
V_c	Cutting speed	F_r, F_ψ, F_κ	Cutting force component along r, ψ and κ

Introduction

5-axis machining strategies are widely used in the manufacturing of sculptured free-form surfaces such as propellers, turbines, and dies/molds. Modeling the cutting forces is the basis for the prediction of tool wear and breakage, machine-tool vibration, cutting parameter optimization and surface quality. To generate G-Code for a specific machine tool, the user have to provide all of the required input parameters such as cutter geometry and material, desired depth of cut, spindle speed, and feed rate. These inputs are often based on handbooks and years of experience. The prediction of cutting forces allows the enhancement of both cutting conditions and tool path but requires precise knowledge of the cutting process. A general model for predicting cutting forces which is based on analytical calculations, is developed for 5-axis machining programs to plan and optimize the machining process.

A literature review shows that there have been many models developed to predict the cutting forces in milling processes. Modeling of cutting can be based on three different and complementary approaches: an analytical approach devoted to describe and use the thermomechanical phenomena occurring during cutting, a mechanistic approach attempting to calculate the cutting forces simply and effectively by using reference measurements transposed to other situations, or a numerical approach usually based on Finite Elements.

Fontaine et al. (2006, 2007) described a complete geometrical model for 3-axis milling and used a thermomechanical oblique cutting model taking into account the part material behaviour and the friction conditions at the tool-chip interface. The capability of this thermomechanical approach for the modelling of other machining processes (turning, drilling and milling) was also demonstrated by Molinari et al (2007).

Vector clipping is a mechanistic method which was proposed in Chappel (1983). In this method, the surface is approximated with a cloud of points and the surface normal vectors are calculated at various points. To simulate the machining process, the intersection of each vector with the tool swept envelope must be calculated.

In the Z-mapping method, the corresponding height of each grid point is stored as a Z-value. For each movement of the tool, Z-values are compared with the tool position and then updated. Anderson (1978) proposed Z-mapping in collision detection and elimination in NC machining. Kim et al. (2003) used the Z-mapping technique to determine the cutter contact area in 3-axis sculptured surface ball-end milling. In Lazoglu's study (2003), Z-mapping is used to determine the chip load. Lee et al. (2002) developed an enhanced Z-mapping method

by applying the supersampling technique. As a result, both efficiency and accuracy of the Z-mapping method were improved. One of the applications of Z-mapping in 5-axis milling is the one presented by Fussel et al. (2003). In that study, tool-workpiece engagement was identified using an extended Z-buffer method. They used the swept envelope of the cutter to determine the intersection between the tool and Z-buffer elements. Also, the 5-axis movement of the tool was approximated as a 3-axis motion by keeping the desired accuracy.

Voxel and Octree are 3D solid discrete methods. Voxel has a simple database. As a result, it is easy and fast to apply. Also, the workpiece stock update can be performed quickly. Karunakaran et al. (2010) applied this method to simulate material removal from the stock in milling operations. Kim et al. (2006) used the Octree method to identify cutting regions in milling operations.

In analytical methods, information on the workpiece geometry is used together with the tool position to analyze and simulate the process geometry. A Book by Shah et al. (1995) presents detailed theory and applications of surface modeling techniques for CAD/CAM of complex surface geometries. One of the analytical studies in 3-axis sculptured surface machining is the one presented by Meng Lim et al. (1995). Another book by Choi et al. (2012) presents detailed theory and applications for 5-axis sculptured surface machining. Du et al. (2005) and Bailey et al. (2002) developed analytical methods to simulate 5-axis tool motion and process geometry. Ozturk et al. (2006) analytically modeled the chip load in ball-end milling of free form surfaces. Lee et al. (2000) estimated the depth of cuts by positioning the tool axis coincident with the surface normal at that point. Imani et al. (1998) modeled the cutter-workpiece engagement boundaries using a geometric simulation system which uses a commercial solid modeler as the geometric engine.

In Zeroudi et al (2010), an analytical model was presented to predict the cutting forces for 3-axis milling. In the present paper, we extend this model to 5-axis milling by using the Cutter Localisation data (CL data) coming from a CAM application to calculate the tool path, orientation and engagement in the workpiece material.

1. Description of the tool trajectory

Fig. 1 shows that the z'-axis is the main axis of the spindle, while θ_{eq} is the angle between the z-axis and the z'-axis which can be either clock-wise or counter clock-wise. The workpiece coordinate system is referenced using capital letters and is denoted *(X, Y, Z)* with *O* as the origin. The z-axis and the *Z*-axis have the same direction but different center point.

In the present study, we consider the displacement of the tool from point *E* to *E'* which is only due to the rotational movements around *X, Y, Z* respectively. As a result, phenomena such as axial eccentricity, deflection and vibrations are not taken into account.

In practice, the origin *O* of the workpiece is palpated by the 5-axis milling machine while the origin *E* of the local coordinate system is obtained by measuring the length of the tool fixed in its holder using a measuring tool apparatus.

Fig. 1 shows that the purchased theoretical surface is formed by a succession of a tilted straight line segments which are created from *CL* points resulting from CAM application. The tilt angle of the tool δ is due to the inclination of the segments forming the trajectory T_k. It can be calculated from $CL_X(i,k)$, $CL_Y(i,k)$ and $CL_Z(i,k)$ as follows:

$$\tan(\delta) = \frac{CL_Z(i+1,k) - CL_Z(i,k)}{\sqrt{\Delta CL_X{}^2 + \Delta CL_Y{}^2}} \quad (1)$$

Where: $\Delta CL_X = CL_X(i+1,k) - CL_X(i,k)$ and $\Delta CL_Y = CL_Y(i+1,k) - CL_Y(i,k)$.

Fig. 1 Schematic representation of the inclination angle δ and the CL point coordinate

2. Tool configuration

2.1 Five-axis milling machine configuration

A 5-axis milling machine refers to a machine's ability to move a tool or a part in five different axes simultaneously. Fig. 2 represents a schematic representation of the tool orientation angles.

Fig. 2 Schematic representation of the swiveling angles θ_n , θ_t , the equivalent angle θ_{eq} and the elliptic deformation angle $\theta_{z'y}$

To calculate the tool position in the global coordinate system, the transformation relationship between the tool coordinate system and the global coordinate system is expressed as follows:

$$\begin{pmatrix} x \\ y \\ z \end{pmatrix}_{xyz} = \begin{bmatrix} \cos(\theta_t) & \sin(\theta_t)\sin(\theta_n) & \sin(\theta_t)\cos(\theta_n) \\ 0 & \cos(\theta_n) & -\sin(\theta_n) \\ -\sin(\theta_t) & \cos(\theta_t)\sin(\theta_n) & \cos(\theta_t)\cos(\theta_n) \end{bmatrix} \begin{pmatrix} x' \\ y' \\ z' \end{pmatrix}_{x'y'z'} \quad (2)$$

Then, the components *(I, J, K)* of the tool carrying axis are obtained via :

$$\begin{pmatrix} I \\ J \\ K \end{pmatrix} = \begin{pmatrix} \sin(\theta_t)\cos(\theta_n) \\ -\sin(\theta_n) \\ \cos(\theta_t)\cos(\theta_n) \end{pmatrix} \quad (3)$$

2.2 The swiveling and the elliptic deformation angle

The swiveling angles indicate the instantaneous tool position in the global coordinate system. In the present study, these angles are known and given by a CAM software in APT format. However, this consideration imposes to express the swiveling angles as a function of *I*, *J* and *K* which are directly extracted from the CL data.

To calculate the tool position in the global coordinate system, the contact between the tool and the machined surface is assumed to be a point. When the spherical part of the tool swivels around its center, it does not generate changes in the global coordinate system. Nevertheless, the change in the orientation of the tool may be observed in its cylindrical part. The two tool orientation angles, which are represented in Fig. 2, describe the tool movement. The first angle θ_n corresponds to a spin around the *x*-axis, while the second angle θ_t corresponding to a spin around the *y*-axis.

The transformation matrix developed in Section 2 is used to express the tool's new position in the global coordinate system. The components of the axis carrying the tool are used to express θ_n and θ_t as a function of *I*, *J* and *K* as follows:

$$\theta_n = \arctan\left(\frac{-J}{\sqrt{I^2+K^2}}\right) \quad \text{and} \quad \theta_t = \arctan\left(\frac{I}{K}\right) \quad (4)$$

The equivalent angle θ_{eq}, which is due to the swiveling angles θ_n and θ_t, can be calculated by using the scalar product and assuming unit vector in the z and z' axes. The expression of θ_{eq} is given as follows:

$$\theta_{eq} = \arccos\left(\cos(\theta_t)\cos(\theta_n)\right) \quad (5)$$

As function of *I*, *J* and *K*, the expression of θ_{eq} so obtained is given as follows:

$$\theta_{eq} = \arctan\left(\frac{K}{\sqrt{1-K^2}}\right) + n\pi \quad (6)$$

As shown in Fig. 2, the elliptical deformation angle $\theta_{z'y}$, which is obtained by projecting the *z*'and *y* axes in the *(x, y)* plane, may be determined as follows :

- If $\theta_n \neq 0$, then: $\theta_{z'y} = \arctan\left(-\frac{\sin(\theta_t)}{\tan(\theta_n)}\right)$ (7)
- If $\theta_n = 0$, then : $\theta_{z'y} = \frac{\pi}{2} + n\pi$ (8)

The final expression of $\theta_{z'y}$ as a function of *I*, *J* and *K*, is given as follows:

- If $\forall I \neq 0$ and $J > 0$, then : $\theta_{z'y} = \tan^{-1}\left(\frac{I}{J}\right)$ (9)
- If $\forall I \neq 0$ and $J < 0$, then : $\theta_{z'y} = \tan^{-1}\left(\frac{I}{J}\right) + \pi$ (10)
- If $I > 0$ and $J = 0$, then : $\theta_{z'y} = \frac{\pi}{2}$ (11)
- If $I < 0$ and $J = 0$, then : $\theta_{z'y} = \frac{3\pi}{2}$ (12)
- If $I = 0$ and $J > 0$, then : $\theta_{z'y} = 0$ (13)
- If $I = 0$ and $J < 0$, then : $\theta_{z'y} = \pi$ (14)

2.3 The influence of swiveling angles

The geometry of the tool is made of two parts. The first part, called the body, is a cylinder of radius R_0 equal to the nominal radius of the second part which is hemispherical. The center of the hemispherical part is denoted *C* and the tip of the tool is denoted *E.*

Fig. 3 The Position of P point influenced by the equivalent angle θ_{eq} in 5-axis configuration

When the tool moves in 3, 4 or 5 axes configuration, the swiveling angles strongly affect the modeling variables such as the current point *P* and the height *z* along the rotation angle (see Fig. 3).

The effect of the swiveling angles can be described via the following points:

- For the 3-axis configuration, the speed is zero at point E, whereas for the 5-axis configuration, the speed is zero at point E'.
- On the ED_1 segment, there is no difference in the volume of removed matter observed for both 3 and 5-axis configurations.
- On the CD_2 segment, with $0 < \theta_{eq} < \pi$, we remain on the spherical part in both configurations and there is no additional matter removed.
- However, on the D_1C segment, with $\pi < \theta_{eq} < 2\pi$, there is an additional quantity of matter removed in the 5-axis configuration, as compared with the quantity removed in 3-axis configuration.

As shown in Fig. 3, the dimensions *EB* and *BC* are calculated from the triangle *CE'B* :

$$EB = \frac{R_0}{\cos(\theta_{eq})} - R_0 \qquad \text{and} \qquad BC = \frac{R_0}{\cos(\theta_{eq})} \tag{15}$$

The dimensions D_1C, CD_2, ED_1, and ED_2 are calculated from the triangles CD_1F_1 and CD_2F_2 with a similar method:

$$D_1C = CD_2 = R_0 \sin(\theta_{eq}),\ ED_1 = R_0\left(1-\sin(\theta_{eq})\right) \text{ and } ED_2 = R_0\left(1+\sin(\theta_{eq})\right) \tag{16}$$

In the interval $\overline{ED_1} \le z < \overline{ED_2}$, the dimensions G_1H_1 and H_2G_2 are deduced from the triangles $F_1G_1H_1$ and $F_2G_2H_2$, respectively:

$$G_1H_1 = H_2G_2 = \left(z - R_0\left(1-\sin(\theta_{eq})\right)\right)\tan(\theta_{eq}) \tag{17}$$

The coordinates (X_P, Y_P, Z_P) of point *P* in the global coordinate system are given by :

$$\begin{pmatrix} X_P \\ Y_P \\ Z_P \end{pmatrix} = \begin{pmatrix} X_E + x_P \\ Y_E + y_P \\ Z_E + z_P \end{pmatrix} \tag{18}$$

2.1.1 Tool penetration

Considering a 5-axis machining process, the penetration of the tool may be calculated for any value of the swiveling angle or the direction of the motion relative to the global coordinate system. As shown in Fig. 3, the z^* may be calculated with the following formula in the interval $\overline{EB} \le z < \overline{EC}$:

$$z^* = R_0 - (R_0 - z)\cos(\theta_{eq}) \tag{19}$$

2.1.2 Tool effective radius R*(z)

For a point *P* located on the envelope of the tool at a machining depth z^* and along the axis of rotation, the corresponding radius $R^*(z)$ of the tool measured in the *(x, y)* plane is as follows:

- If $\overline{EB} \le z \le \overline{EC}$, then: $R^*(z) = \sqrt{R_0^2 - \left((R_0 - z)\cos(\theta_{eq})\right)^2}$ (20)
- If $z > \overline{EC}$, then: $R^*(z) = R_0$ (21)

3. Position of the current point *P* along the cutting edge

The current point *P* is located on a cutting edge in the local frame *(x', y', z')* with coordinates (x'_P, y'_P, z'_P) for a given tooth *j* and an altitude *z'*. The following expression gives the coordinates of *P* in the global coordinate system :

$$\begin{pmatrix} x_P \\ y_P \\ z_P \end{pmatrix} = \begin{bmatrix} \cos(\theta_t) & \sin(\theta_t)\sin(\theta_n) & \sin(\theta_t)\cos(\theta_n) \\ 0 & \cos(\theta_n) & -\sin(\theta_n) \\ -\sin(\theta_t) & \cos(\theta_t)\sin(\theta_n) & \cos(\theta_t)\cos(\theta_n) \end{bmatrix} \begin{pmatrix} R^*(z)\sin(\psi_j^*(z)) \\ R^*(z)\cos(\psi_j^*(z)) \\ z^* \end{pmatrix} \tag{22}$$

When the tool is oriented in a given direction, it forms an ellipse or a half-ellipse with the machined surface, depending on the equivalent angle θ_{eq}. Fig. 4 illustrates different marks in the penetration process between the tool and a plane surface.

Fig. 4 Envelope of the tool forming an elliptic section with the horizontal plane caused by the swiveling angles

4.1 The current point position in the circular part

Considering the circular part of the trace, for each case displayed in Fig. 5 (a), (b), (c), (d), where: $\theta_{z'y} - \frac{\pi}{2} \le \psi_j(z) \le \theta_{z'y} + \frac{\pi}{2}$, the coordinates of the current point *P* must be written in the local frame *(x,y,z)* using the transformation matrix given by the following expression:

$$\begin{pmatrix} x_P \\ y_P \\ z_P \end{pmatrix} = \begin{pmatrix} R(z)\sin(\psi_j(z)) \\ R(z)\cos(\psi_j(z)) \\ z \end{pmatrix} \quad (23)$$

Where $R(z)$ and $\psi_j(z)$ are expressed as follows :

$$R(z) = \sqrt{R^{*2}(z) - (R_0 - z)^2 \sin^2(\theta_{eq})} \quad (24)$$

$$\psi_j(z) = \arctan\left(\frac{\cos(\theta_t) x'_P + \sin(\theta_t)\sin(\theta_n) y'_P + \sin(\theta_t)\cos(\theta_n) z'_P}{\cos(\theta_n) y'_P - \sin(\theta_n) z'_P} \right) \quad (25)$$

Fig. 5 (a) Envelope of the tool in the (x, y) plane for $0 \le \theta_{z'y} \le \frac{\pi}{2}$

Fig. 5 (b) Envelope of the tool in the (x, y) plane for $\frac{\pi}{2} \le \theta_{z'y} \le \pi$

Fig. 5 (c) Envelope of the tool in the (x, y) plane for $\pi \le \theta_{z'y} \le \frac{3\pi}{2}$

Fig. 5 (d) Envelope of the tool in the (x, y) plane for $\frac{3\pi}{2} \le \theta_{z'y} \le 2\pi$

4.2 The current point position in the elliptical part

Fig. 5 (a), (b), (c), (d) show that the elliptical part starts to be observed when $z > z_F$. Using the same method as in previous section, for $\theta_{z'y} + \frac{\pi}{2} \le \psi_j(z) \le \theta_{z'y} + \frac{3\pi}{2}$, the coordinates of the current point *P* are calculated as follows :

$$\begin{pmatrix} x_P \\ y_P \\ z_P \end{pmatrix} = \begin{pmatrix} (R(z_F) + G_1H_1)\cos(\theta_{z'y} - \psi_j(z))\sin(\theta_{z'y}) - R(z)\sin(\theta_{z'y} - \psi_j(z))\cos(\theta_{z'y}) \\ (R(z_F) + G_1H_1)\cos(\theta_{z'y} - \psi_j(z))\cos(\theta_{z'y}) + R(z)\sin(\theta_{z'y} - \psi_j(z))\sin(\theta_{z'y}) \\ z \end{pmatrix} \quad (26)$$

Here, z_F, $R(z_F)$ and G_1H_1 are expressed as follows :

$$z_F = ED_1 = R_0(1 - \sin(\theta_{eq})) \quad (27)$$

$$R(z_F) = \sqrt{R_0^2 - (R_0 - z_F)^2} \quad (28)$$

$$G_1H_1 = (z - R_0(1 - \sin(\theta_{eq})))\tan(\theta_{eq}) \quad (29)$$

4. Tool engagement

The engagement of the tool in the matter must be determined in order to know the quantity of matter machined by each tooth. For each cutting edge, it is necessary to determine the position of the current point *P* and project it onto the uncut surface attacked by the tooth. This surface is delimited by three types of boundary conditions:

- The relative position of the workpiece uncut surfaces along the three axes and specifically along the Z-axis (upper initial or pre-form surface).
- The previous tool path considered without any tool deflection and with perfect surface finish (path interval *Δp* defined in *(X, Y)* plane, see Fig. 1).
- The path of the previous tooth.

5.1 Description of the tool contact

As shown in Fig. 6 (a), from the point *P* we draw a normal unit vector denoted $\vec{n}$, which is perpendicular to the vector $\vec{f}$ defined as the instantaneous advance vector.

Fig. 6 (a) Parameters describing the contact between the tool and the machined surface,
(b) Feed angles φ_x and φ_z

Both position vector $\vec{n}$ and point *P* depend on the orientation of the z'-axis, which allows optimizing the inclination of the tool regarding the surface, thus avoiding a contact between the tip of the tool (low cutting speed zone) and the machined surface.

To calculate the position of points *C* and *E'* in the global coordinate system (*X, Y, Z*), the vectors $\overrightarrow{OC}$ and $\overrightarrow{OE'}$ are expressed as follows:

$$\overrightarrow{OC} = \overrightarrow{OP} + R_0.\vec{n} \qquad \text{and} \qquad \overrightarrow{OE'} = \overrightarrow{OC} - R_0.\vec{z}' \tag{30}$$

As shown in Fig. 6 (b), the vector $\vec{f}$ can be calculated using the φ_x and φ_z angles or using the advance by tooth between two successive *CL* points. the vector $\vec{f}\left(f_x, f_y, f_z\right)$ may be also expressed in the global coordinate system using the following expression:

$$\begin{pmatrix} f_x \\ f_y \\ f_z \end{pmatrix} = \begin{pmatrix} CL_x(i+1,k) - CL_x(i,k) \\ CL_y(i+1,k) - CL_y(i,k) \\ CL_z(i+1,k) - CL_z(i,k) \end{pmatrix}_{(x,\,y,\,z)} \tag{31}$$

5.2 Engagement compared to the trace of the preceding tooth

In the case of non-deformed chip, the trace left by the preceding tooth is taken into account in the calculation of the chip thickness t_0^*. For that, two successive positions of the tool are considered along an elementary toolpath.

The trajectory of the preceding tooth is often necessary to model radial eccentricity because of its high influence on the cutting forces. If the eccentricity $\vec{e}$ is less than the feed per tooth $\vec{f}_t^{\,*}$ (which is reasonable), the non-deformed chip thickness t_0^* can be obtained from the following scalar product.

$$t_0^* = \vec{f}_t^{\,*}\vec{e}_r^{\,*} + \left(\vec{e}_j^{\,*} - \vec{e}_{j-1}^{\,*}\right)\vec{e}_r^{\,*} \tag{32}$$

where:

- $\vec{e}_r$ is the normal vector at the tool envelope at point *P*.
- $\vec{e}_j$ is the vector of eccentricity for tooth *j*.
- $\vec{e}_{j-1}$ is the vector of eccentricity for tooth *j-1*.

5. Cutter geometry discretization

As shown in Fig. 7, a spherical coordinate system $(\vec{e}_r^*, \vec{e}_\kappa^*, \vec{e}_\psi^*)$ is associated to point *P* to define the position of any elementary edge on the envelope of the tool. $\vec{e}_r^*$ is the unit vector orthogonal to the envelope of the tool, which is opposite to the unit vector $\vec{n}$. $\vec{e}_\kappa^*$ is the unit vector corresponding to the κ^* angle displacement, and $\vec{e}_\psi^*$ is the unit vector corresponding to the angular displacement ψ. The plane P_0 is the orthogonal to the envelope of the tool, P_n is the normal plane to the cutting edge and P_t is the tangent plane to the envelope of the tool.

Fig. 7 Geometry and discretization of the elementary cutting edge for a cutter swell

6.1 The angle of location κ^*

As shown in Fig. 7, the angle of location κ represents the angular displacement between $\vec{e_r}$ and $\vec{z}$. The angle κ varies along the envelope of the tool as follows:

- If $\overline{EB} \le z \le \overline{EC}$, then: $\kappa^* = \cos^{-1}\left(\cos(\theta_{eq})\left(\frac{1-z}{R_0}\right)\right)$ 33
- If $z > \overline{EC}$, then: $\kappa^* = \frac{\pi}{2}$ 34

6.2 Local helix angle $i^*(z)$

From Fig. 7, the expression of the local helix angle $i^*(z)$ is as follows:

$$i^*(z) = \arctan\left(\frac{R^*(z)}{R_0}\tan(i)\right) \quad 35$$

6.3 Tangent vector $\vec{t}^*$

From Fig. 7, the projection of the tangent vector to the edge $\vec{t}^*$ in the spherical coordinate system $(\vec{e}_r^*, \vec{e}_\kappa^*, \vec{e}_\psi^*)$ gives the following expression:

$$\vec{t}^* = -\cos(\lambda_s^*)\vec{e}_\kappa^* + \sin(\lambda_s^*)\vec{e}_\psi^* \quad 36$$

6.4 The angle λ_s^* and the relation between α_0^* and α_n^*

From Fig. 7, we can deduce the expression of λ_s^* and the relation between the orthogonal cutting angle α_0^* and the normal cutting angle α_n^*:

$$\tan(\lambda_s^*) = \tan(i^*)\sin(\kappa^*) \quad 37$$

$$\tan(\alpha_n^*) = \tan(\alpha_0^*)\cos(\lambda_s^*) \quad 38$$

6.5 The elementary cutting width dw^*

From Fig. 7, The expression of the elementary cutting width dw^* is as follows:

$$dw^* = \frac{dz^*}{\sin\left(\kappa^*\right)} \tag{39}$$

6.6 Angular position on the helicoidal edge ψ_j^*

The angular position of the running point *P* on a given tooth *j* is is given by a formula similar to the one used in peripheral milling. As a result, the variation in angular position $\Delta\psi$ changes with position along the considered helix as shown in Fig. 8. the expression for ψ_j^* is as follows:

$$\psi_j^* = \theta^* - \Delta\psi^* + \left(j-1\right)\frac{2\pi}{N_t} \tag{40}$$

Fig. 8 Angular position in the (x, y) plane

6.7 Shift angle $\Delta\psi^*$

From Fig. 8, the expression of the shift angle $\Delta\psi^*$ relative to the tip of the tool is as follows:

$$\Delta\psi^* = \left[1 - \frac{\left(R_0 - z\right)\cos\left(\theta_{eq}\right)}{R_0}\right]\tan\left(i\right) \tag{41}$$

Based on the assumption that the helix stepover is constant along the tool, both expressions (40) and (41) are valid along the tool. This assumption is an approximation, and amounts to considering the inclination angle of the edge constant along the helix. In practice, cutters of constant stepover are more widespread, and this is why this approximation is acceptable.

6.8 Total rotation of the tool θ^*

The rotation of the tool is locally propagated and the angle of rotation between two successive *CL* points can be easily determined from the local interpolation segment, the feed per tooth f_t and the local feed angle φ_z. The total rotation of the tool between two successive points *CL* is noted $\Delta\theta^*(i)$ and may be calculated for each step as follows:

$$\Delta\theta^*(i) = \frac{2\pi}{N_t}\left(\frac{\left|CL_X(i+1,k) - CL_X(i,k)\right|}{f_t\cos\left(\varphi_z\right).\left[\cos\left(\theta_t\right).\cos\left(\theta_n\right)\right]}\right) \tag{42}$$

Here, θ^* is equal to the summation of the $\Delta\theta^*(i)$'s, which are calculated for each elementary displacement along the tool trajectory.

6. Tool engagement in the previous machined surface

7.1 Height of previous machined surface (z_{sp})

To consider, as simply as possible, the engagement of the tool in the previous machined surface at distinct height *z* values during a series of machining passes, it is enough to compare the position of the current point *P* with those of the preceding trajectories. The previous surface can be described in a precise way using the peak error method or an approximate way which considers the previous surface as perfect.

The simplest idea is to consider a plane surface but in the case of a more complex surface, the upper surface can be described starting from the preceding nominal surface while

considering no defects in the resulting surface. Point P is in a position of cut if $z_P \leq z_{sp}$, where z_{sp} is the height of the preceding surface corresponding to $x = x_P$ and $y = y_P$.

Fig. 9 Parameters defining the trajectory of the tool for a rectilinear advance in the (X, Y, Z) plane, (case of upright machining)

The height of the previous machined surface z_{sp} can be calculated by the transversal inclination angle $\varphi_{\Delta p}$, which represents the slope of the machined surface in the transversal direction of the advance, as shown in Fig. 9 and Fig. 10.

The calculation of the transverse inclination angle $\varphi_{\Delta p}$ and the height of preceding surface z_{sp} are the same as for the case of 3-axis milling. The expressions are as follows:

$$\varphi_{\Delta p} = \tan^{-1}\left(\frac{\left(CL_Z(i,k) - CL_Z(i,k-1)\right)\cos\left(\varphi_z\right)}{CL_Y(i,k) - CL_Y(i,k-1)}\right) \quad 43$$

$$z_{sp} = \left|\frac{d_n}{\cos\left(\varphi_z\right)} - \frac{R_0}{\cos\left(\varphi_z\right)} + R_0\right| + \left(x_P\cos\left(\varphi_x\right) + y_P\sin\left(\varphi_x\right)\right)\tan\left(\varphi_z\right) + \left(-x_P\sin\left(\varphi_x\right) + y_P\cos\left(\varphi_x\right)\right)\tan\left(\varphi_{\Delta p}\right) \quad 44$$

Fig. 10 Schematic of z_{sp} coordinates in the local reference frame

7.2 Calculation of point C_P

The transverse offset between two successive tool paths in the plane *(X, Y)* corresponds to the pitch Δp. As shown in Fig. 12, the point C_p is the intersection between the axis of the tool and the preceding trajectory of the tool in the *(X, Y)* plane, independently from the current point P and the height ($Z = Z_P$). The preceding trajectory of tool is considered perfect without any influence of the tool eccentricity. At point C_p, the radius of the tool envelope is denoted R_P. The current point P is in position of cut if $\left|PC_P\right| \geq R_P$.

Fig. 11 Comparison between point P on tooth j and the previous tool path for a straight path in the plane (X, Y) at $Z = Z_P$ with $\Delta p > 0$

The distance PC_P is calculated by the same method as in 3-axis milling case. The distance in absolute value is given by the following exression:

$$\left|PC_P\right| = \sqrt{\left(X_{CP} - X_P\right)^2 + \left(Y_{CP} - Y_P\right)^2} \quad 45$$

7.3 Calculation of the radius R_P

The position of P point in the *(X, Y)* plane is denoted *CL,* and its height Z_{CL_P} .The calculation of CL_P on the $T_{k\text{-}1}$ trajectory remains unchanged compared to the case of 3-axis milling. When machining up or down, the height Z_{CL_P} on *the* $T_{k\text{-}1}$ trajectory can be calculated as follows:

$$Z_{CL_P} = CL_Z(i,k-1)\left[1 - \left(\frac{X_{C_P} - CL_X(i,k-1)}{CL_X(i+1,k-1) - CL_X(i,k-1)}\right)\right] + CL_Z(i+1,k-1)\left(\frac{X_{C_P} - CL_X(i,k-1)}{CL_X(i+1,k-1) - CL_X(i,k-1)}\right) \quad 46$$

In 5-axis milling, it is necessary to calculate the position of P and C_P points along the preceding trajectory $T_{k\text{-}1}$ in order to calculate the radius R_P.

Fig. 12 Different cases for the tool position

R_P can then be calculated by distinguishing the cases illustrated in Fig. 12 :

- Case 1 : If $Z_P < \left(Z_{CLp} - R_0\right)$, then: $R_P = 0$
- Case 2.1 : If $(Z_{CLp} \geq Z_P \geq \left(Z_{CLp} - R_0\right)$ and $Z_P \geq Z_F)$, then the calculation for $\theta_{z'y} - \frac{\pi}{2} \leq \psi_j(z) \leq \theta_{z'y} + \frac{\pi}{2}$ gives the following expression :

$$R_P = \sqrt{\left(R\left(z_{F(T_{k-1})}\right) + G_1H_{1(T_{k-1})}\right)^2 \cos^2\left(\theta_{z'y} - \psi_{j(T_{k-1})}(z_P)\right) + R^2_{(T_{k-1})}(z_P)\sin^2\left(\theta_{z'y} - \psi_{j_{(T_{k-1})}}(z_P)\right)} \quad 47$$

With:

$$Z_{F(T_{k-1})} = ED_1 = R_0\left(1 - \sin(\theta_{eq})\right)$$

$$R(z_{F_{(T_{k-1})}}) = \sqrt{R_0{}^2 - \left(R_0 - R_0\left(1 - \sin\left(\theta_{eq}\right)\right)\right)^2}$$

$$G_1H_1 = \left(z - R_0\left(1 - \sin\left(\theta_{eq}\right)\right)\right)\tan\left(\theta_{eq}\right)$$

$$R_{(T_{k-1})}(z_P) = R_P = \sqrt{\left|\left(Z_{CLp} - Z_P\right)^2 - R_0^2\right|}$$

$$\psi_{j_{(T_{k-1})}}(z_P) = \frac{\pi}{2} + \varphi_x = \frac{\pi}{2} + \arctan\left(\frac{CL_Y(i+1,k-1) - CL_Y(i,k-1)}{CL_X(i+1,k-1) - CL_X(i,k-1)}\right)$$

- Case 2.2 : If $(Z_{CLp} \geq Z_P \geq \left(Z_{CLp} - R_0\right)$ and $Z_P < Z_F)$, then the calculation for $\theta_{z'y} + \frac{\pi}{2} \leq \psi_j(z) \leq \theta_{z'y} + \frac{3\pi}{2}$ gives the following expression:

$$R_P = \sqrt{\left|\left(Z_{CLp} - Z_P\right)^2 - R_0^2\right|} \quad 48$$

7. Radial tool eccentricity

Tool eccentricity is a shift between the axis of rotation of the spindle and the central axis of the tool. There are two types of eccentricity: (a) axial eccentricity which is the angular shift between the axis of the tool and the axis of the spindle, and (b) radial eccentricity which is the the distance between the axis of the tool and the axis of the spindle.

Radial eccentricity is modeled by a value of eccentricity denoted *e*. As shown in Fig. 13 (a), the angle ψ_e^* is in the *(x', y')* plane, considering the first tooth *(j = 1)* as a reference tooth in the direction of the tool's rotation for $z' = 0$. C_f is the center of the tool at the height z_P, $C_f = E'$ when $z' = 0$, and C_R is the projection of C_f on the z'-axis of spindle. The vector $\overrightarrow{C_fC_R}$ is defined as the vector of eccentricity and is denoted $\vec{e}$. When $\vec{e}$ is colinear with the y'-axis, $\theta^* = 0°$ is the referential angular position of the cutter. Fig. 13 (b) shows an intermediate position of the current point *P* located in the local frame *(x, y, z)* with coordinates (x_P, y_P, z_P) along the edge $j = 1$ with $\theta^* > 0$.

Fig. 13 Schematic representation of radial eccentricity:
(a) When $\theta^* = 0°$, **(b)** When $\theta^* > 0°$

The angular position ψ_j^* of the current point *P* on the edge *j* at the height z_P must be modified compared to the case without disturbances. The new expression is given as follows:

$$\psi_j^*(z_P) = \left(\theta^* + \psi_e^*\right) - \Delta\psi^* + (j-1)\frac{2\pi}{N_t} \quad 49$$

where $\Delta\psi^*$ is the shift angle defined in formula (41).

Since the eccentricity does not change with tool orientation, $\vec{e}^{\,*} = \vec{e}$, and the local frame *(x', y', z')* is not centered anymore at the point *E'* defined above, the coordinates of *P* point are calculated as follows:

$$\begin{pmatrix} x_P \\ y_P \\ z_P \end{pmatrix} = \begin{bmatrix} \cos(\theta_t) & \sin(\theta_t)\sin(\theta_n) & \sin(\theta_t)\cos(\theta_n) \\ 0 & \cos(\theta_n) & -\sin(\theta_n) \\ -\sin(\theta_t) & \cos(\theta_t)\sin(\theta_n) & \cos(\theta_t)\cos(\theta_n) \end{bmatrix} \begin{pmatrix} R^*(z)\sin(\psi^*_j) + e^*\sin(\theta^*) \\ R^*(z)\cos(\psi^*_j) + e^*\cos(\theta^*) \\ z^* \end{pmatrix} \quad 50$$

Due to the radial eccentricity of the tool, the equivalent radius $Re^*(z_P)$ at *P* point must be calculated in order to deduce the local cutting speed V_{ce}. In the (x', y') plane, *P'* is the perpendicular projection of point *P* on the $\overrightarrow{C_f C_R}$ vector, as shown in Fig. 14 and the following relation is obtained:

$$R_e^*(z_P) = \sqrt{R^*(z_P)^2 + (e)^2 + 2eR^*(z_P)\cos\left(\psi_e^* - \Delta\psi^* + (j-1)\frac{2\pi}{N_t}\right)} \quad 51$$

Then, V_{ce} is calculated using the following relation :

$$V_{ce} = R_e^*(z_P)\Omega \quad 52$$

To be more rigourous, the cutting speed direction is also variable, and that also affects the angles α^*_n et λ^*_s angles along the considered elementary edge. This does not affect significantly the cutting forces. Therefore, there is no real interest in taking into account such a consideration.

In the *(x', y', z')* frame, the normal vector $\vec{e}_r$ and the vectors of eccentricity $\vec{e}_j$ and $\vec{e}_{j-1}$ are calculated as follows :

$$\begin{aligned} \vec{e}_r^* &= \sin(\psi^*_j)\sin(\kappa^*)\vec{x}' + \cos(\psi^*_j)\sin(\kappa^*)\vec{y}' - \cos(\kappa^*)\vec{z}' \\ \vec{e}_j^* &= e\sin(\theta^*)\vec{x}' + e\cos(\theta^*)\vec{y}' \\ \vec{e}_{j-1}^* &= e\sin(\theta^* - 2\pi/N_t).\vec{x}' + e\cos(\theta^* - 2\pi/N_t)\vec{y}' \end{aligned} \quad 53$$

8. Global forces on the tool

Starting from the local geometry (shear angle ϕ^*, edge tilt angle λ^*_s, elementary cutting width dw^* and thickness of the non-deformed chip t_0^*) for each elementary cutting edge, an estimate of the local cutting forces ($d\vec{F}_r$, $d\vec{F}_\kappa$ and $d\vec{F}_\psi$) can be calculated using either a mechanistic (based on the empirical coefficients of cut) or a thermomechanical method (based on a constitutive law and friction parameters).

In order to simplify and optimize the computing time in the calculation of the cutting forces along the trajectory of the tool**,** the following considerations were taken during the calculations:

- Calculations are made for each *CL* point during a rotation of the tool of $2\pi/N_t$ (N_t is the number of teeth of the tool) ;
- The result obtained in a *CL* point can be reproduced throughout the distance between the point considered *CL(i, k)* and the following point *CL(i+1, k)* ;

- The elementary cutting forces $d\vec{F}_r$, $d\vec{F}_\kappa$ and $d\vec{F}_\psi$ are calculated for each edge engaged in the workpiece ($t_0^* > 0$) for a given angular position θ^* and expressed in the $(\vec{e}_r^*, \vec{e}_\kappa^*, \vec{e}_\psi^*)$ frame.

Fig. 14 Schematic of elementary cutting forces associated to local frames at P and P' points

The transformation matrices are used to express the elementary cutting forces in the *(x', y', z')* and *(X, Y, Z)* coordinate systems respectively. The calculations are given in the following expressions:

$$\begin{pmatrix} dF_{x'}(\theta^*, z^*, j) \\ dF_{y'}(\theta^*, z^*, j) \\ dF_{z'}(\theta^*, z^*, j) \end{pmatrix} = \begin{pmatrix} \sin(\psi^*{}_j)\sin(\kappa^*) & \sin(\psi^*{}_j)\cos(\kappa^*) & \cos(\psi^*{}_j) \\ \cos(\psi^*{}_j)\sin(\kappa^*) & \cos(\psi^*{}_j)\cos(\kappa^*) & -\sin(\psi^*{}_j) \\ -\cos(\kappa^*) & \sin(\kappa^*) & 0 \end{pmatrix} \begin{pmatrix} dF_r(\theta^*, z^*, j) \\ dF_\kappa(\theta^*, z^*, j) \\ dF_\psi(\theta^*, z^*, j) \end{pmatrix} \quad 54$$

and

$$\begin{pmatrix} dF_x(\theta^*, z^*, j) \\ dF_y(\theta^*, z^*, j) \\ dF_z(\theta^*, z^*, j) \end{pmatrix} = \begin{bmatrix} \cos(\theta_t) & \sin(\theta_t)\sin(\theta_n) & \sin(\theta_t)\cos(\theta_n) \\ 0 & \cos(\theta_n) & -\sin(\theta_n) \\ -\sin(\theta_t) & \cos(\theta_t)\sin(\theta_n) & \cos(\theta_t)\cos(\theta_n) \end{bmatrix} \begin{pmatrix} dF_{x'}(\theta^*, z^*, j) \\ dF_{y'}(\theta^*, z^*, j) \\ dF_{z'}(\theta^*, z^*, j) \end{pmatrix} \quad 55$$

The cutting forces $d\vec{F}_x$, $d\vec{F}_y$ and $d\vec{F}_z$ can be calculated for the elementary cutting forces for each considered tooth, using the following expression:

$$\begin{pmatrix} dF_x(\theta^*, z^*) \\ dF_y(\theta^*, z^*) \\ dF_z(\theta^*, z^*) \end{pmatrix} = \begin{pmatrix} \sum_{j=1}^{N_t} dF_x(\theta^*, z^*, j) \\ \sum_{j=1}^{N_t} dF_y(\theta^*, z^*, j) \\ \sum_{j=1}^{N_t} dF_z(\theta^*, z^*, j) \end{pmatrix} \quad 56$$

Finally, another summation is made for each elementary disc in the height range considered, taking into account the 5-axis milling conditions. The following expression gives the values of $\vec{F}_x$, $\vec{F}_y$ and $\vec{F}_z$ in the global coordinate system, which can be compared later with the experimental results obtained by using a load cell :

$$\begin{pmatrix} F_x(\theta^*) \\ F_y(\theta^*) \\ F_z(\theta^*) \end{pmatrix} = \begin{pmatrix} \sum_{z=0}^{R_0} dF_x(\theta^*, z^*) \\ \sum_{z=0}^{R_0} dF_y(\theta^*, z^*) \\ \sum_{z=0}^{R_0} dF_z(\theta^*, z^*) \end{pmatrix} \quad 57$$

Conclusion

This article proposes an analytical method for modeling the cutting forces in 5-axis milling of sculptured surfaces by extending an existing approch developed for 3-axis milling. This model is based on the use of CL data coming from a CAM application to calculate the tool path, the orientation angle, the spindle speed and the discernement of workpiece-tool contact,

from the point of view of the elementary quantity of removed matter along the trajectory of the tool.

To predict cutting forces in the 5-axis milling process, the calculations are performed in this order:

- Orientation angles in the local and the global coordinates systems ;
- Trace of the tool engagement in the machined surface ;
- Height of the current point ;
- Global forces on the tool.

The model developed in the present paper could serve as a theoretical basis to optimize 5-axis milling in order to improve surface finish, tool life, stability and productivity by optimising cutting conditions, tool path, tool-workpiece contact and even tool geometry.

Ethical approval
Not applicable.

Consent to participate
All authors consent to participate to this manuscript.

Consent to publish
All authors consent to publish this manuscript.

Authors' contributions
ZN developed the model for 3-axis milling process. HY extended the model to 5-axis milling process, and wrote this manuscript. LR helped to calculate formulas for the 5-axis milling model.

Funding
Not applicable.

Competing interests
The authors declare that they have no competing interests.

Availability of data and materials
Not applicable.

References

Fontaine, M., Devillez, A., Moufki, A., & Dudzinki, D. (2006). Predictive force model for ball-end milling and experimental validation with a wavelike form machining test. *International Journal of Machine Tools and Manufacture, 46*, 367–380.

Fontaine, M., Moufki, A., Devillez, A., & Dudzinki, D. (2007). Modeling of cutting forces in ball- end milling with tool–surface inclination, Part I: Predictive force model and experimental validation. *Journal of Materials Processing Technology, 189*, 73–84.

Molinari, A., & Moufki, A. (2005). A new thermomechanical model of cutting applied to turning operations, Part I: Theory. *International Journal of Machine Tools and Manufacture, 45*, 166–180.

Chappel, I.T. (1983). Use of vectors to simulate material removed by NC milling. *Computer-Aided Design, 15*, 156–158.

Anderson, R.O. (1978). Detecting and eliminating collisions in NC machining. *Computer-Aided Design, 10*, 231–237.

Kim, G.M., Kim, B.H., & Chu, C.N. (2003). Estimation of cutter deflection and form error in ball-end milling processes. *International Journal of Machine Tools and Manufacture, 43*, 917–924.

Lazoglu, I. (2003). Sculpture surface machining: a generalized model of ball-end milling force system. *International Journal of Machine Tools and Manufacture, 43*, 453–462.

Lee, S.K., & Ko, S.L. (2002). Development of simulation system for machining process using enhanced Z map model. *Journal of Materials Processing Technology, 130–131*, 608–617.

Fussel, B.K., Jerard, R.B. & Hemmett, J.G. (2003). Modeling of cutting geometry and forces for 5-axis sculptured surface machining. *Computer-Aided Design, 35*, 333–346.

Karunakaran, K.P., Shringi, R., Ramamurthi, D., & Hariharan, C. (2010). Octree-based NC simulation system for optimization of feed rate in milling using instantaneous force model. *International Journal of Advanced Manufacturing Technology, 46*, 465–490.

Kim, Y.H., & Ko, S.L. (2006). Improvement of cutting simulation using the octree method. *International Journal of Advanced Manufacturing Technology, 28*, 1152–1160.

Shah, J.J. & Mäntylä, M. (1995). Parametric and feature-based CAD/CAM: concepts, techniques and applications. *Wiley-Interscience*.

Meng Lim, E.E., Feng, H.Y., Menq, C.H., & Lin, Z.H. (1995). The prediction of dimensional error for sculptured surface productions using the ball-end milling process, Part 1: Chip geometry analysis and cutting force prediction. *International Journal of Machine Tools and Manufacture, 35*, 1149–1169.

Choi, B.K., & Jerard, R.B. (2012). Sculptured surface machining: theory and applications. *Springer Science and Business Media*.

Du, S., Surmann, T., Webber, O. & Weinert, K. (2005). Formulating swept profiles for five-axis tool motions. *International Journal of Machine Tools and Manufacture, 45*, 849–861.

Bailey, T., Elbestawi, M.A., El-Wardany, T.I. & Fitzpatrick, P. (2002). Generic Simulation Approach for Multi-Axis Machining, Part 1: Modeling Methodology. *Journal of Manufacturing Science and Engineering, 124*, 624–633.

Ozturk, B., & Lazoglu, I. (2006). Machining of free-form surfaces. Part I: Analytical chip load. *International Journal of Machine Tools and Manufacture, 46*, 728–735.

Lee, T. S., & Lin, Y. J. (2000). A 3D predictive cutting-force model for end milling of parts having sculptured surfaces. *International Journal of Advanced Manufacturing Technology, 16*, 773–783.

Imani, B.M., Sadeghi, M.H., & Elbestawi, M.A. (1998). An improved process simulation system for ball-end milling of sculptured surfaces. *International Journal of Machine Tools and Manufacture, 38*, 1089–1107.

Zeroudi, N., Fontaine, M., & Necib, K. (2010). Prediction of cutting forces in 3-axis milling of sculptured surfaces directly from CAM tool path. *Journal of Intelligent Manufacturing, 23*, 1573–1587.

Figures

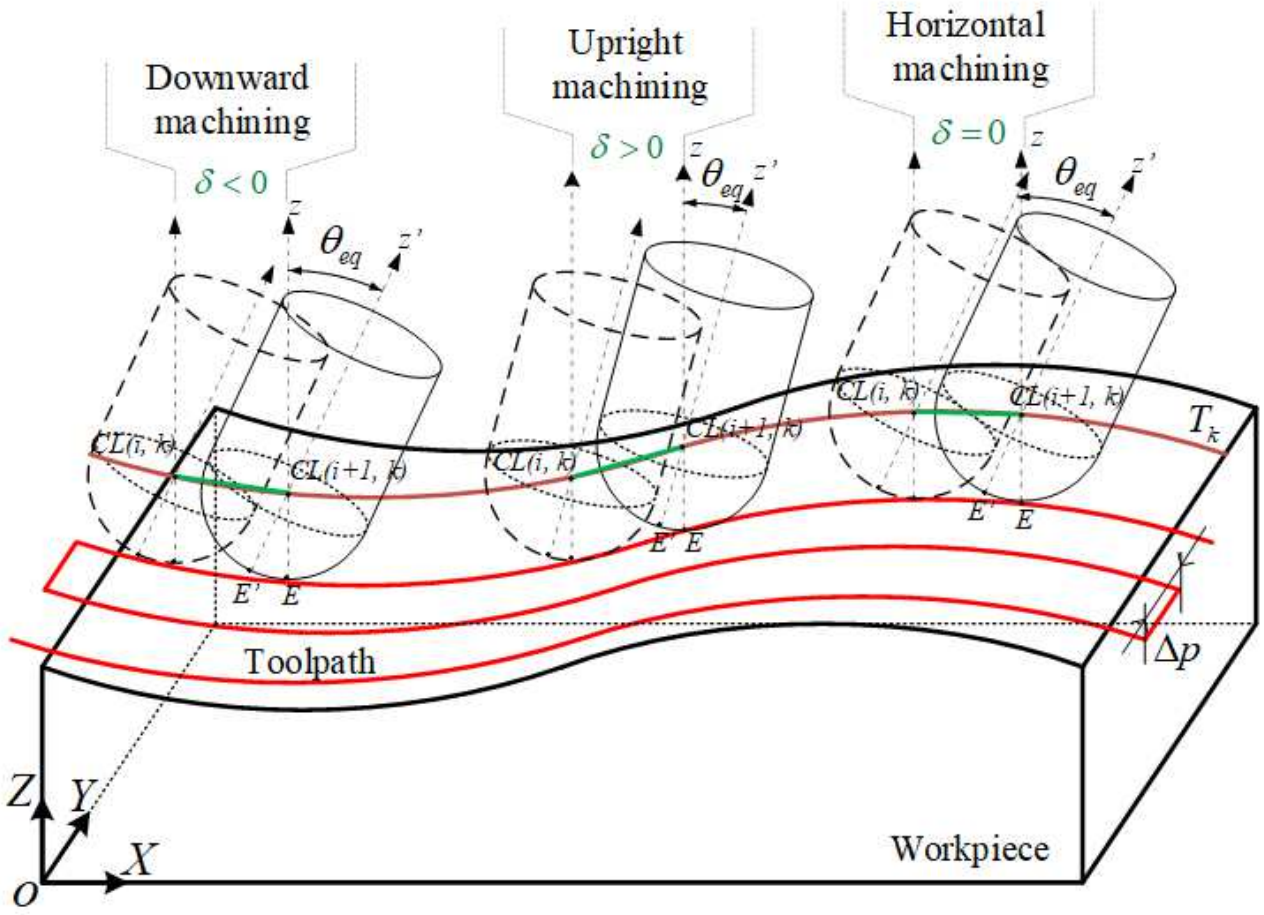

Figure 1

Schematic representation of the inclination angle δ and the CL point coordinate

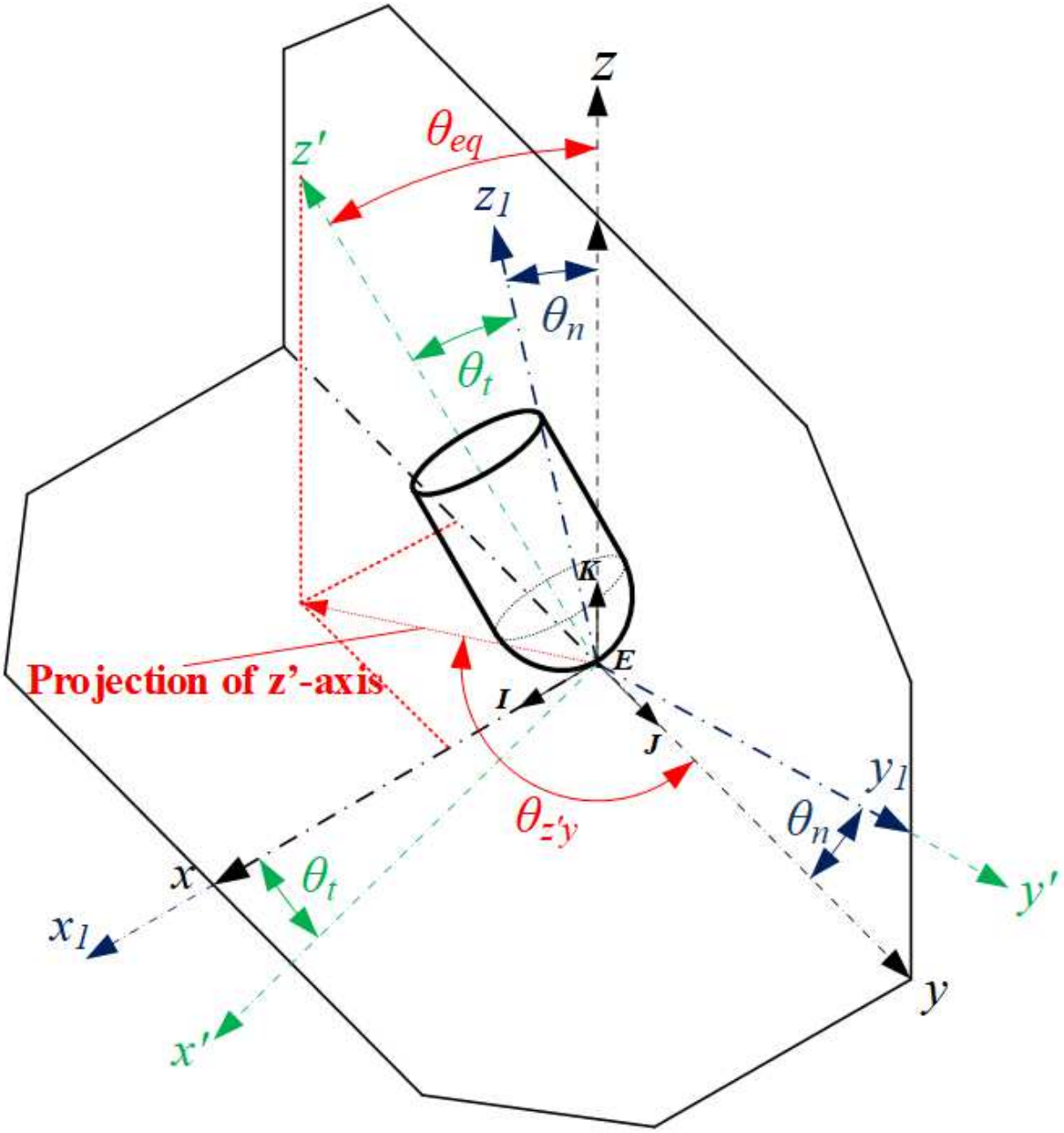

Figure 2

Schematic representation of the swiveling angles θn , θt , the equivalent angle θeq and the elliptic deformation angle θz'y

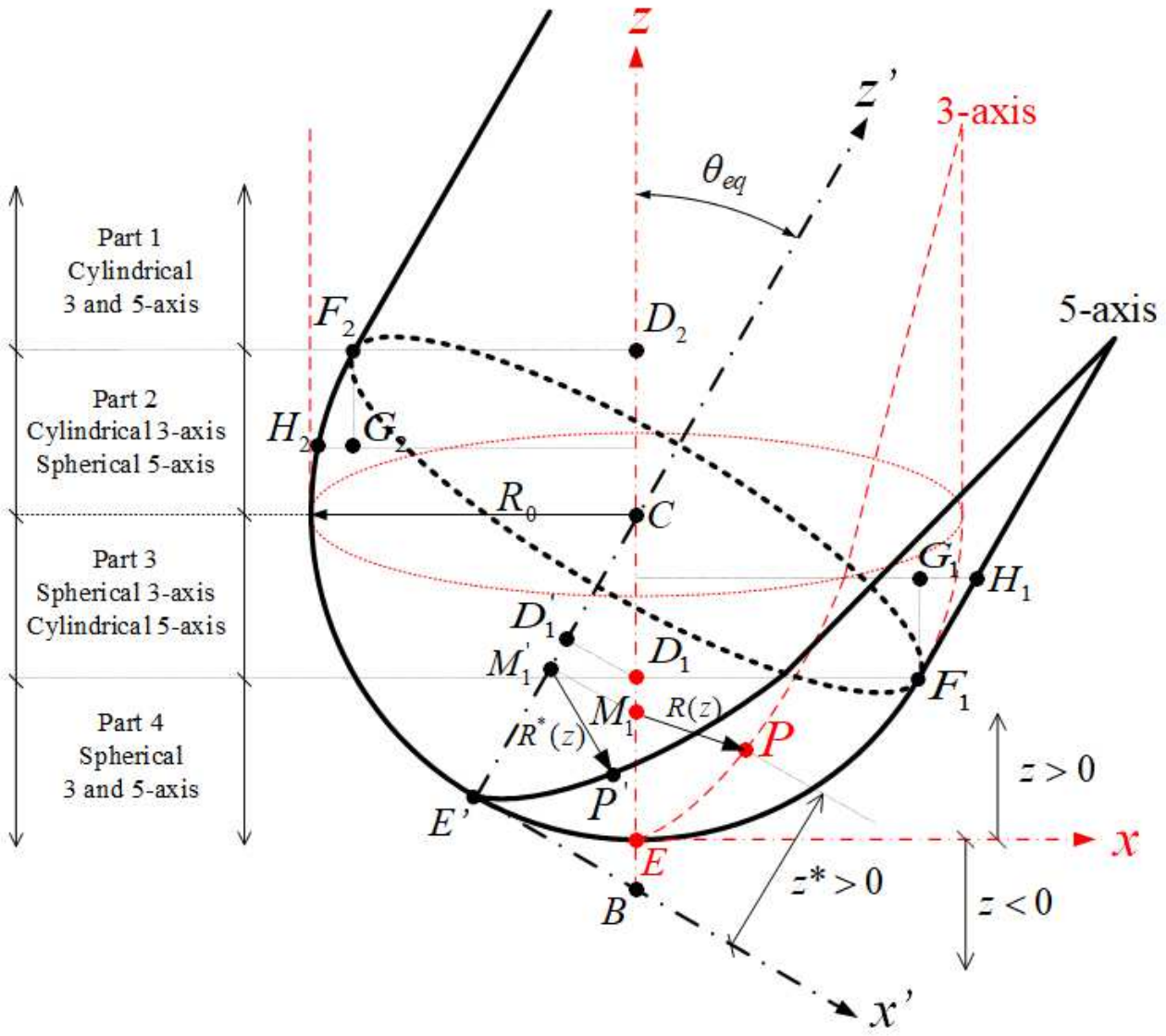

Figure 3

The Position of P point influenced by the equivalent angle θeq in 5-axis configuration

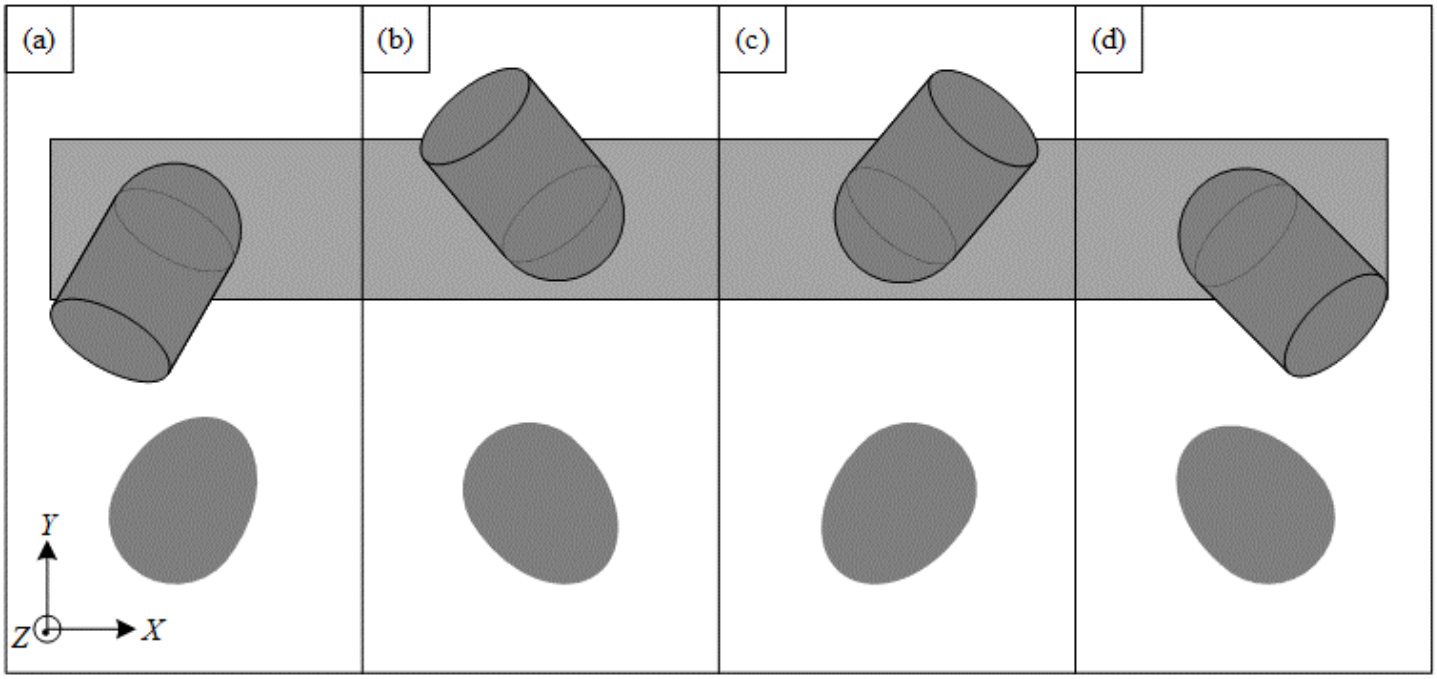

Figure 4

Envelope of the tool forming an elliptic section with the horizontal plane caused by the swiveling angles

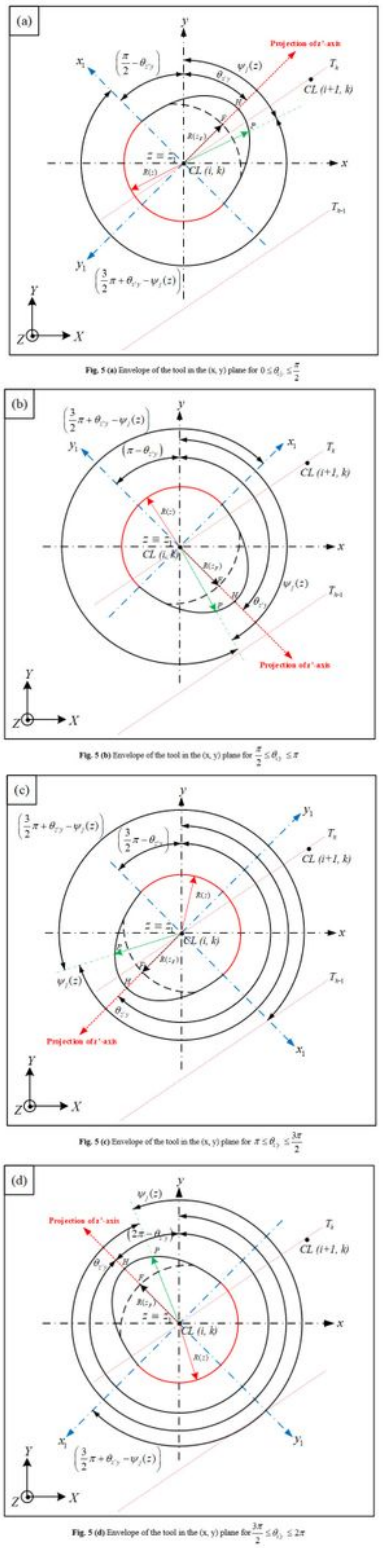

Figure 5

Please see the Manuscript PDF file for the complete figure caption.

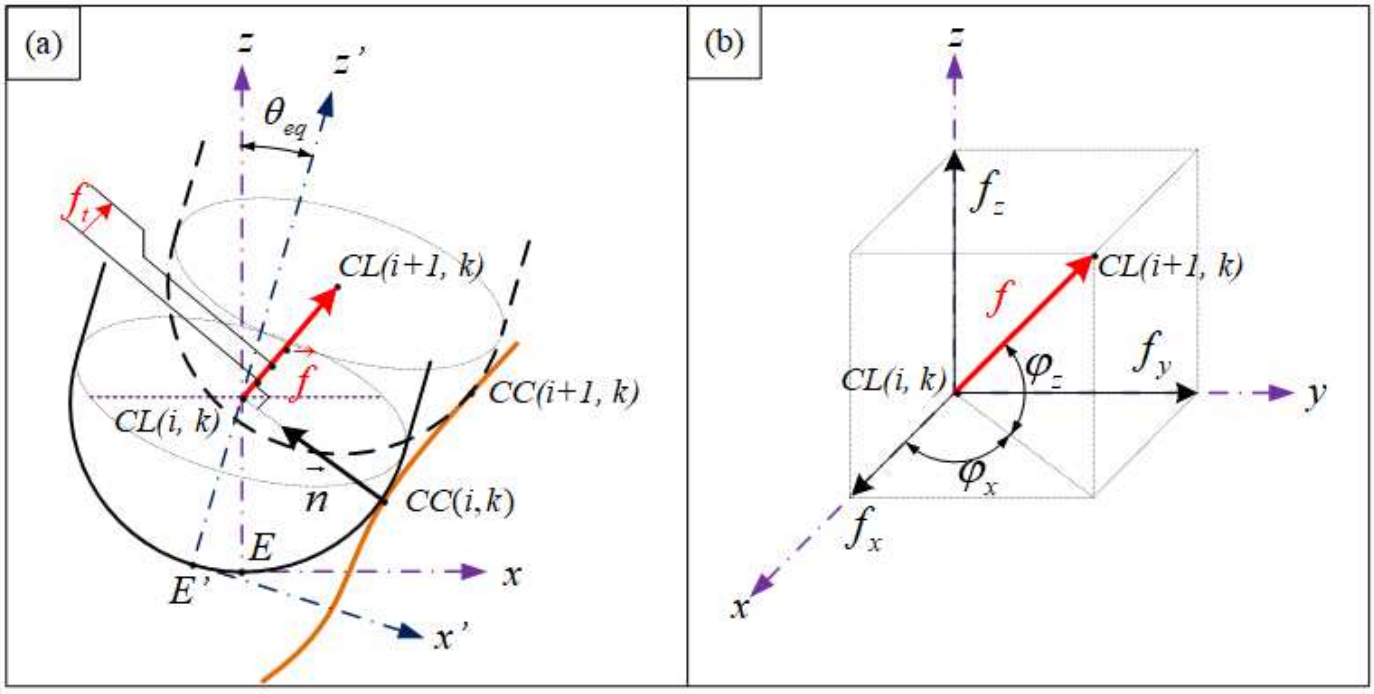

Figure 6

(a) Parameters describing the contact between the tool and the machined surface, (b) Feed angles φx and φz

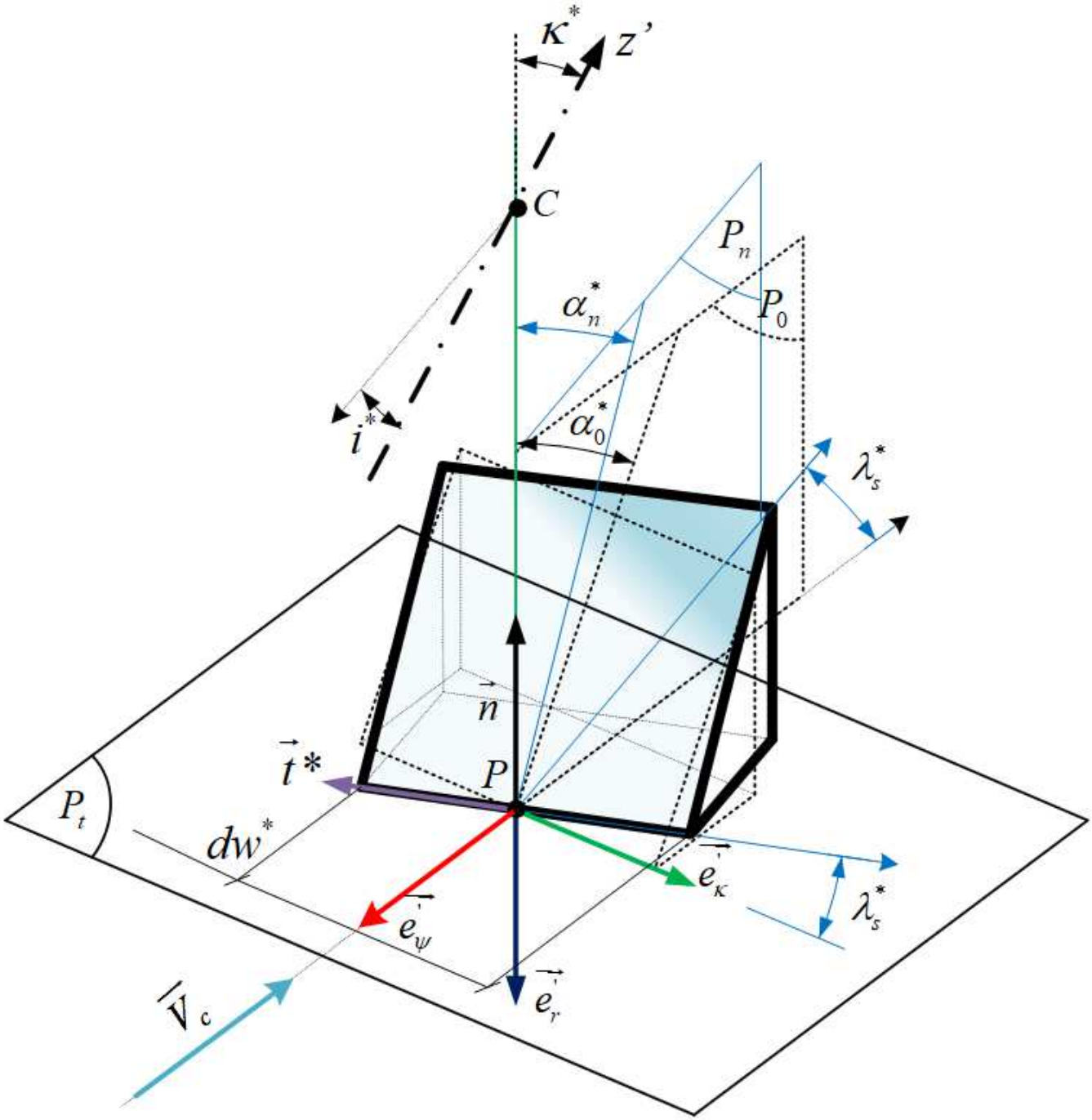

Figure 7

Geometry and discretization of the elementary cutting edge for a cutter swell

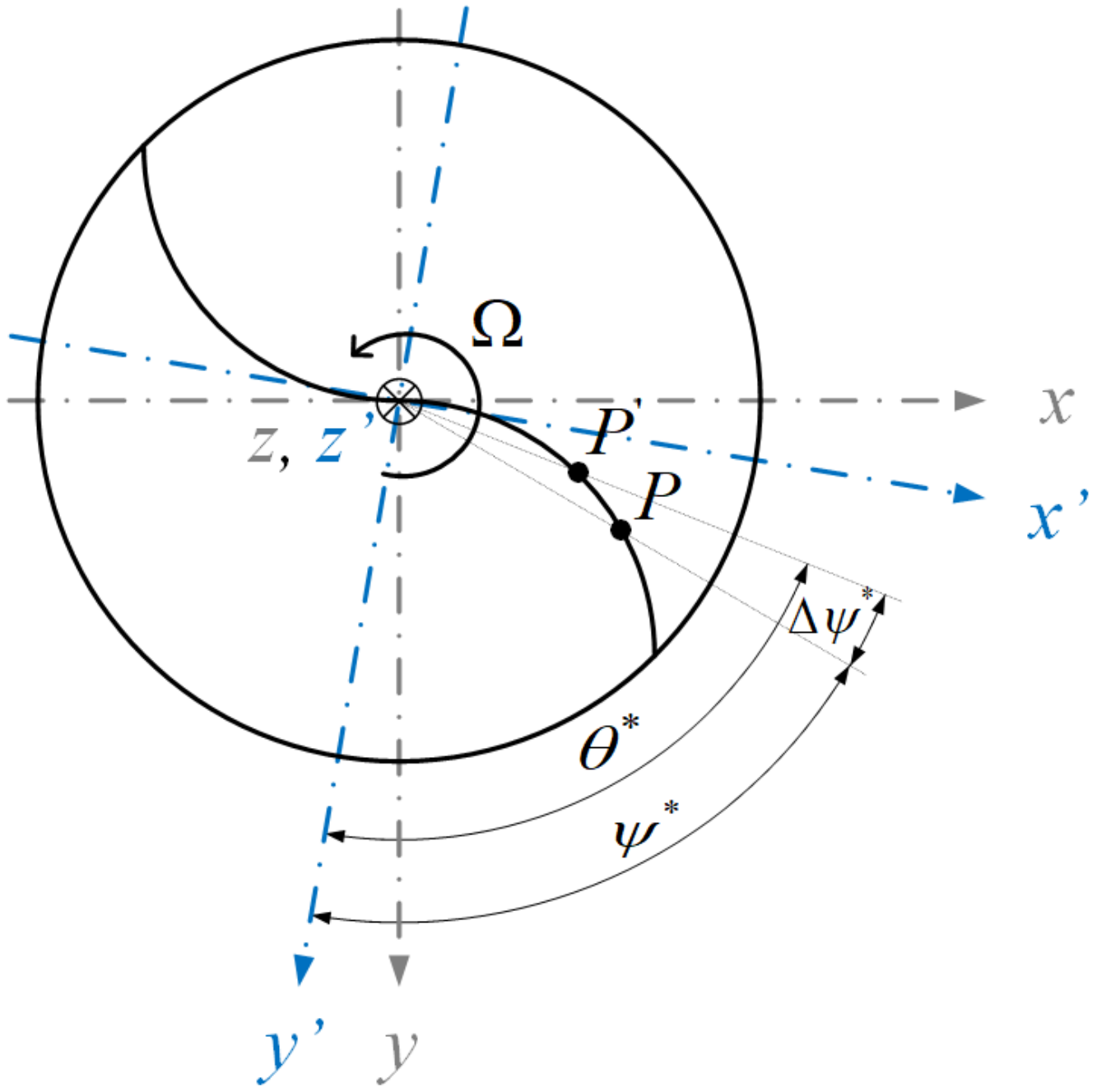

Figure 8

Angular position in the (x, y) plane

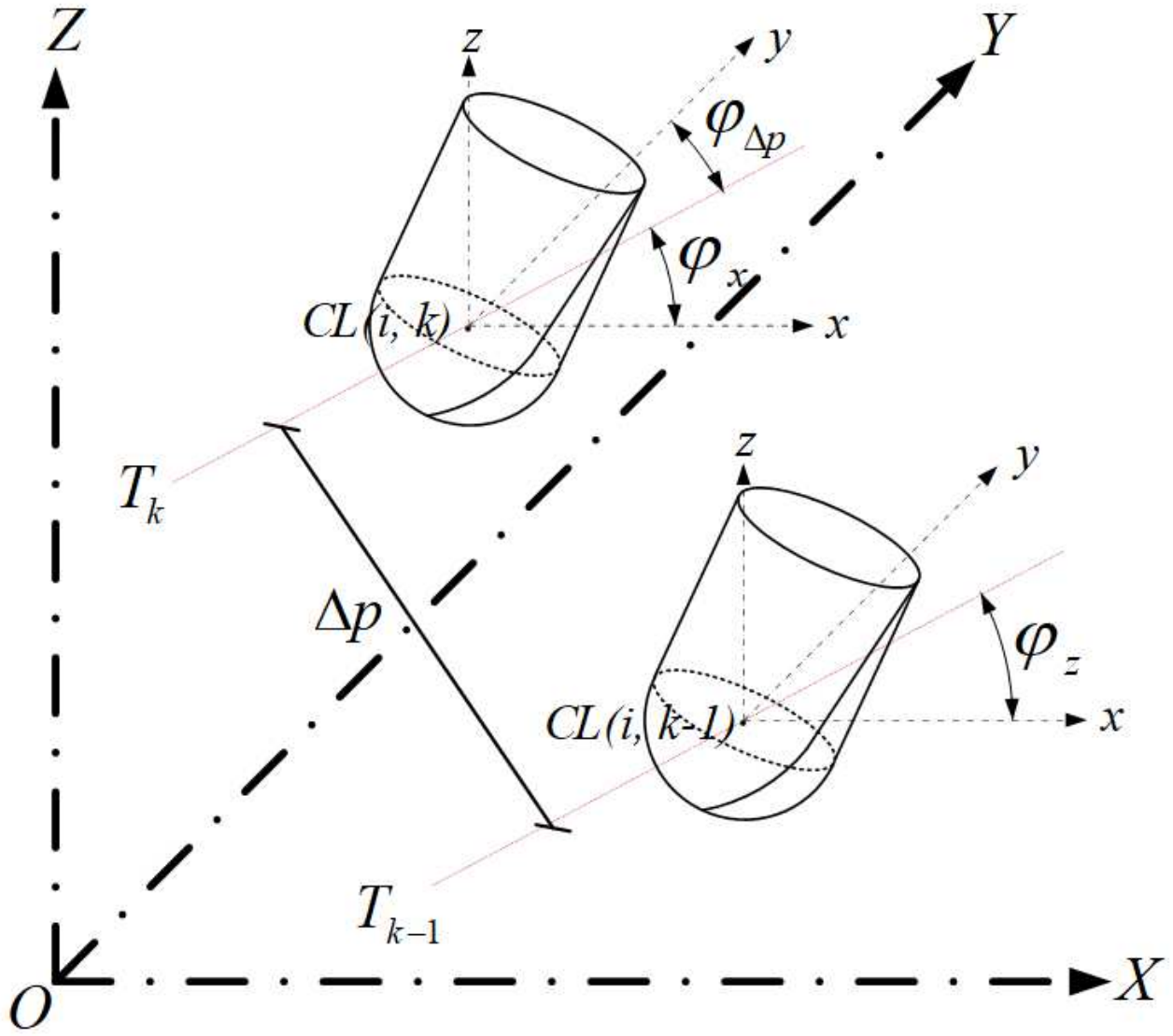

Figure 9

Parameters defining the trajectory of the tool for a rectilinear advance in the (X, Y, Z) plane, (case of upright machining)

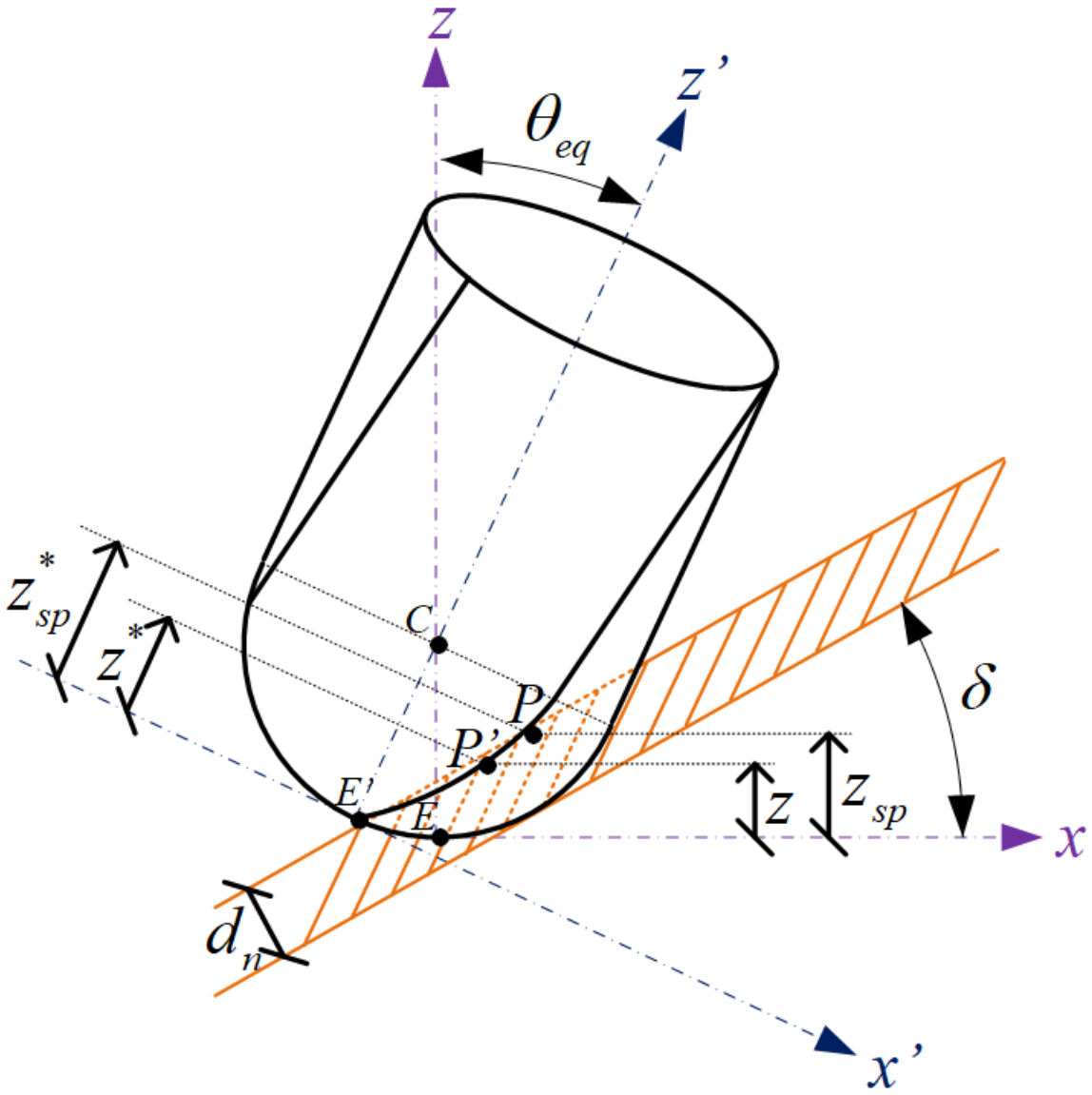

Figure 10

Schematic of zsp coordinates in the local reference frame

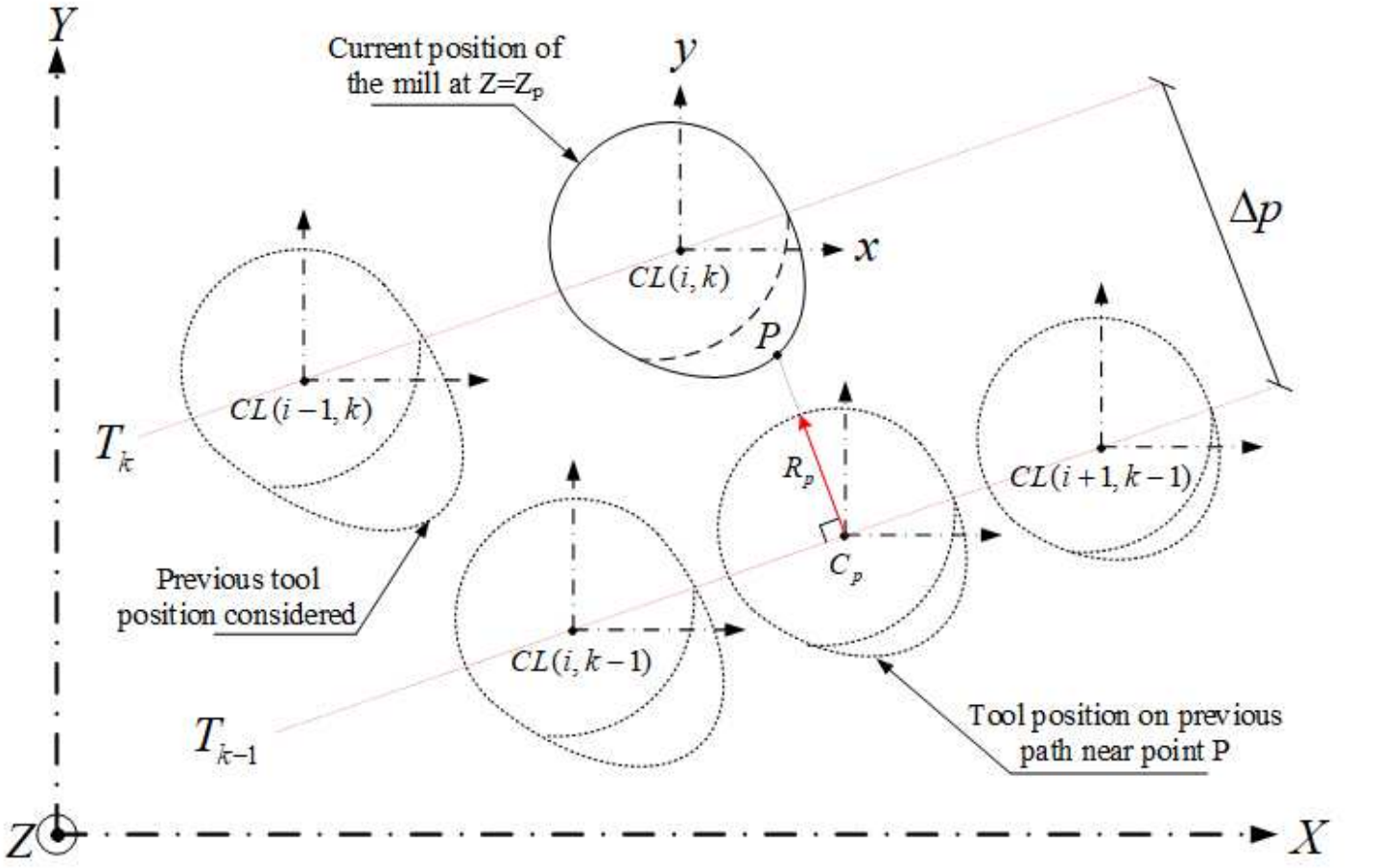

Figure 11

Comparison between point P on tooth j and the previous tool path for a straight path in the plane (X, Y) at Z = ZP with Δp> 0

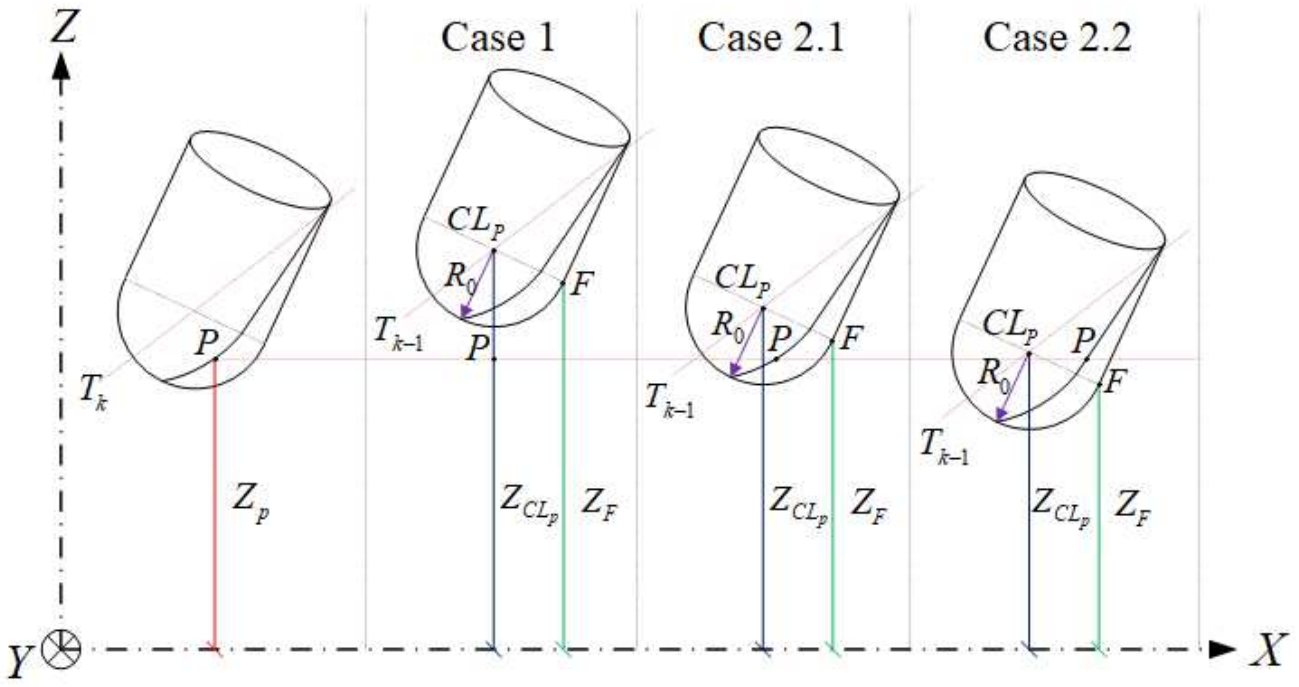

Figure 12

Different cases for the tool position

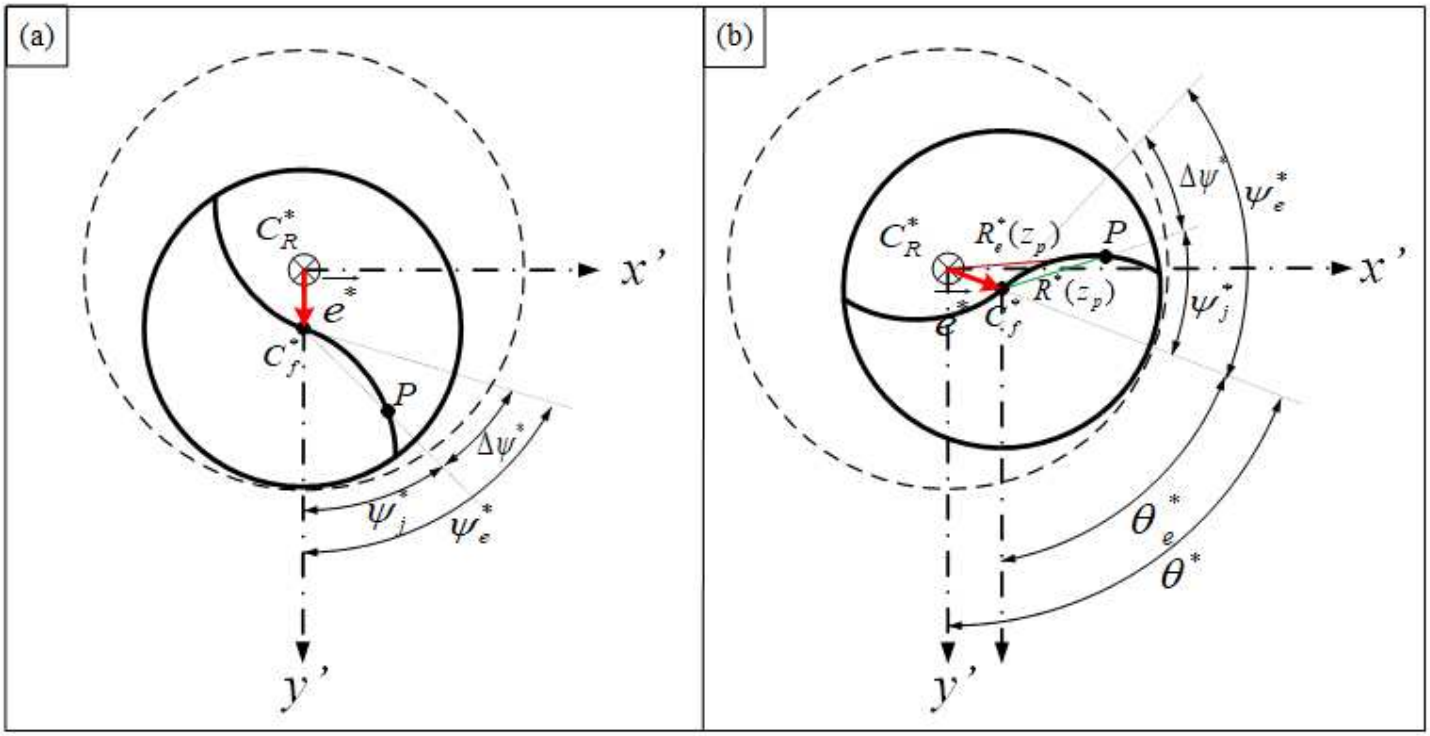

Figure 13

Schematic representation of radial eccentricity: (a) When θ* = 0°, (b) When θ*>0°

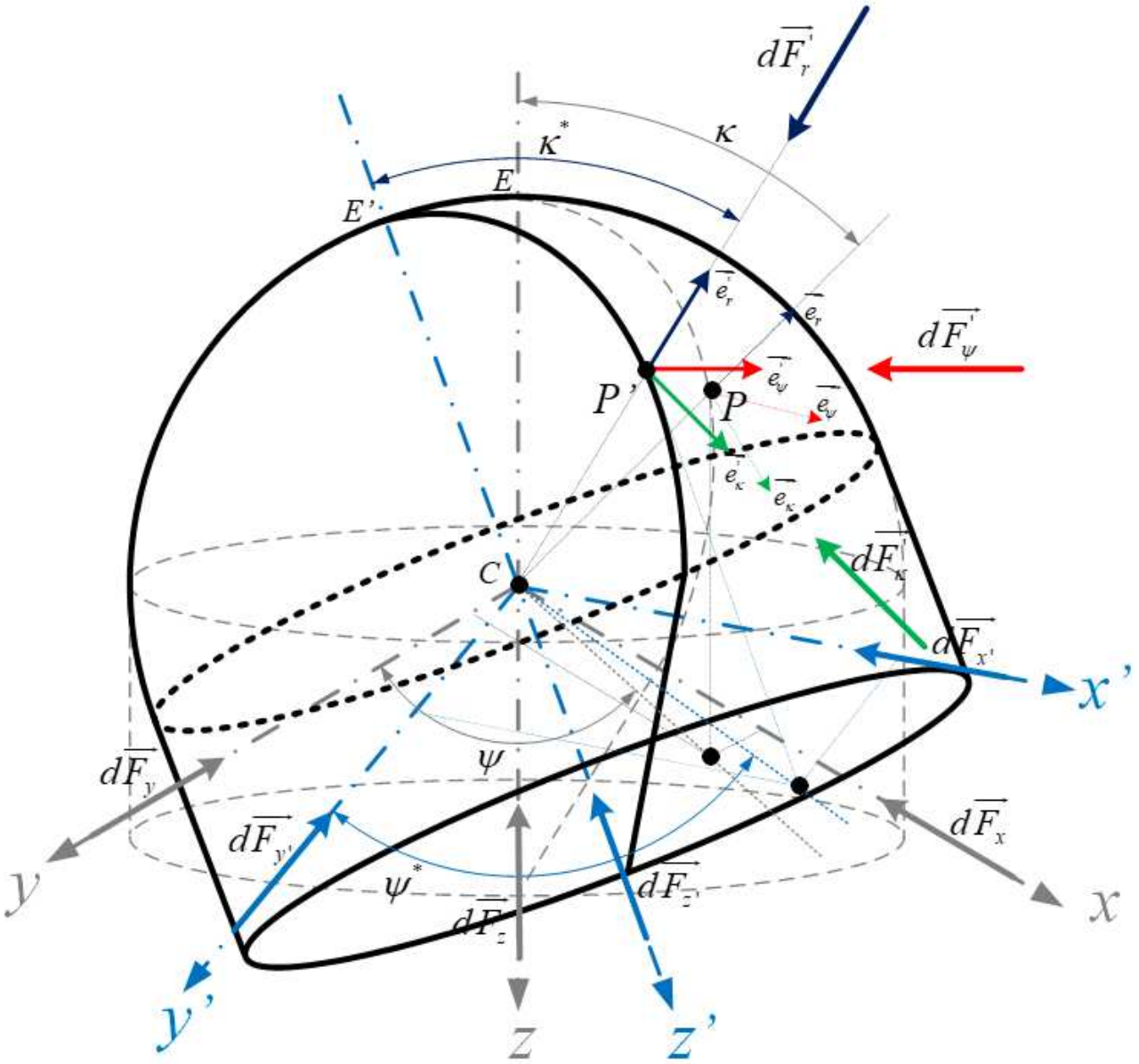

Figure 14

Schematic of elementary cutting forces associated to local frames at P and P' points